sciendo

Nordic Concrete Federation

ISSN online 2545-2819
ISSN print 0800-6377

DOI: 10.2478/ncr-2019-0015

Received: Sept. 15, 2019
Revision received: Dec. 20, 2019
Accepted: Dec. 20, 2019

Width and Edge Beam Effects on the Ultimate Behaviour of RC Bridge Overhangs

José Javier Veganzones – MSc with Licentiate degree
Division of Structural Engineering and Bridges, KTH Royal Institute of Technology, Brinellvägen 23, SE-100 44, Stockholm
jjvm@kth.se

Costin Pacoste – Adjunct Professor
Division of Structural Engineering and Bridges, KTH Royal Institute of Technology, Brinellvägen 23, SE-100 44, Stockholm.
Chief Technical Officer, ELU Konsult, Valhallavägen 117, SE-115 31 Stockholm
costin.pacoste@byv.kth.se

Raid Karoumi – Professor
Head of the Division of Structural Engineering and Bridges, KTH Royal Institute of Technology, Brinellvägen 23, SE-100 44, Stockholm
raid.karoumi@byv.kth.se

ABSTRACT

The bearing capacity of RC overhangs under concentrated loads can be dependent on the width of the slab. The goal of this paper is to investigate the effect of different widths using tests from the literature and non-linear FE-simulations as a reference. Shear force redistributions along the loading process and the shear concrete capacity are analysed. The shear effective width and the influence of an edge beam are also addressed. The results show that the bearing capacity of RC overhangs increase with the width until a transition area is reached and the increase flattens. An increased shear distribution sideways and posterior redistributions under the loading process are enabled. The shear capacity of concrete increases with the width and for loads close to the root an

arch effect is observed. The edge beam contributes to a further increase of the ultimate capacity for wide enough overhangs. The effect of the width and the edge beam is not only quantitative but also qualitative since the failure mode and the critical section are influenced. Existing formulation for shear effective widths should be revisited. Experimental tests used for this purpose should consider wide enough specimens to capture the real behaviour of a bridge overhang slab.

Key words: Overhang slab, Bearing capacity, Width, Edge beam, Shear force, FE-modelling.

1. INTRODUCTION

1.1 General

Shear bearing capacity in RC overhang slabs (Figure 1) has been a research topic in the latest years. A recent study published by the authors [1] investigated the influence of the edge beam in overhang slabs using the experimental tests carried out by Vaz Rodrigues [2] as a reference. The specimen had a width (W) of 10 m and an overhang span (s) of 2.74 m but no edge beam. Thus, numerical simulations were used to investigate the influence of this member. Once a non-linear FE-model was validated against the test results, an edge beam was added to the simulation.

The edge beam contributed to an increase of 15% in the bearing capacity (V) for four concentrated loads placed near the free edge. For loads placed close to the root, the influence was more limited. The relative distance of the load to the root and to the edge beam hence became a relevant factor. Since the edge beam deformed longitudinally to transfer the shear forces from the loads, W might be significant too. If the specimen is not provided with enough W the edge beam would move as a rigid body and its contribution to V, regardless of the load position, could be assumed negligible. Note that in this paper, V will be identified as appropriate with either the failure load in the experiment Q_{exp} or in the numerical FE-simulation Q_{FEM} or the theoretical shear capacity Q_{Rd}.

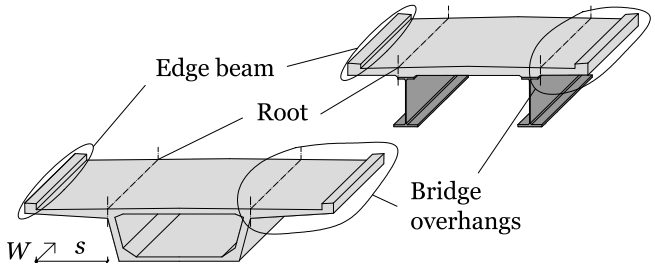

Figure 1 – Overhang slabs with an edge beam in a concrete box-girder and composite bridge

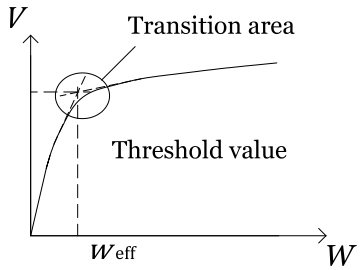

Figure 2 – Increasing V until a threshold value (w_{eff}) is reached

Bearing this in mind, apart from the issue of having or not an edge beam, a related research question is the influence of W on V of overhang slabs. Obviously, this discussion concerns the borderline between beam and slab behaviour. Research studies [3, 4] showed that V on slabs with different support conditions increases significantly with W until a transition area is reached from where such increase flattens, as represented in Figure 2. Within this area, a threshold could be identified and related to the effective width for shear force (w_{eff}) which is defined as the width that is effectively distributing the shear forces from concentrated load(s) at a certain cross section. The suitability of the formulae for its derivation has been questioned [4, 5]. Although the scope

of those research studies did not include overhang slabs of varying W, the authors hypothesize that a similar trend according to Figure 2 is followed.

In this context, the investigation of the mechanisms behind the increase of V with W is of interest. The authors' assumption is that the shear forces from concentrated load(s) are not only transferred in the transversal direction of the bridge towards the root of the overhang, but in the longitudinal direction as well, especially once the bending cracks at the clamped edge are formed. This would imply that for overhang slabs with a short W this redistribution in the longitudinal direction is very limited because cracks appear along the whole root, resulting in a lower V.

This discussion is also related to the evaluation of the shear concrete capacity (v_{Rd}). The fact that the formulation in the Eurocode [6] is empirically based on beam experiments and does not consider flexure-shear interaction while both ACI [7] and Model Code [8] do has been criticized [9]. v_{Rd} could increase due to the flexure-shear interaction since the bending moment in slabs is of lower magnitude compared to beams. Thus, flexural cracks at the root in slabs are not as severe as in beams for the same loading, resulting in a higher depth of the concrete compression chord.

Consequently, the relationship between V and W is not only quantitative but also qualitative. The variation of W may affect the crack pattern, the failure mechanism and the ductility of it. Depending on the load position and the geometry, a transition between flexural and shear failure may occur (Figure 3), and even the critical section for any of those may shift. Moreover, an edge beam may influence the collapse since it affects the shear force distribution and the crack pattern.

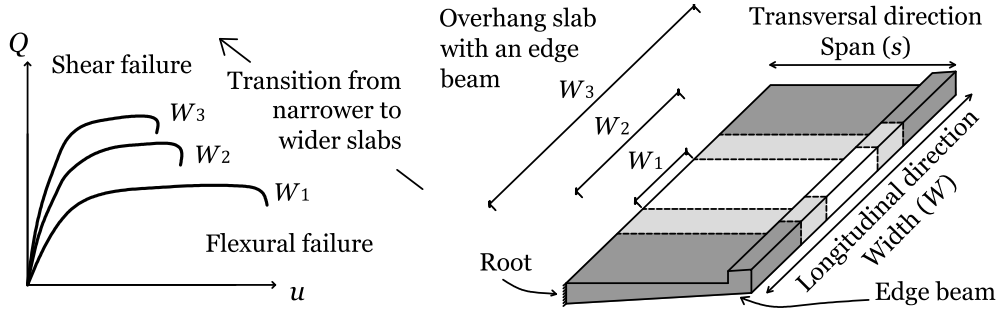

Figure 3 – Failure transition considering overhang slab of different widths

To the authors' knowledge, no comprehensive work addresses the aforementioned factors, which is the novelty of the present study. The aim is to provide a deeper insight into the structural behaviour of RC overhang slabs with/without edge beams under concentrated loads. The goal is to demonstrate that V of the overhang slab increases with W due to a force redistribution in the longitudinal direction and is also influenced by an edge beam. The objectives are the following:

- To validate the non-linear FE-analyses of experimental tests carried out in the literature and use those to investigate different W for overhang slabs with and without an edge beam.
- To demonstrate that the shear force redistribution in the longitudinal direction depends on W and display its evolution throughout the loading process.
- To investigate if an increase of v_{Rd}, if any, is related to an increased W given different values of the shear span ratio (a/d) and, if so, quantify this growth.
- To show that the efficiency of the edge beam distributing shear forces that lead to an increased V depends on W and the proximity of the load to the longitudinal free edge, and propose a parameter to be used as a reference for this and in future work.
- To prove that W and the edge beam influence the failure mode of the overhang slab.

- To confront the obtained results in the light of the existing formulae on w_{eff} and the consideration of failure cross sections studied.

2. LITERATURE BACKGROUND

Classical formulae in the literature to calculate w_{eff} and the control sections that may apply are presented in Figure 4. a_v is the distance to the load edge to the root, b is the load width, d is the effective depth, and t and t_{p} are the thicknesses of the slab and of the pavement respectively.

French [4] – Control Section S0, SI

$$w_{\text{F}} = 2a_v + 2b_y + b_x \leq W \quad (1)$$

French-Dutch [5] – Control Section S0, SI

$$w_{\text{K}} = 2a_v + b_y + b_x \leq W \quad (2)$$

Dutch [4] – Control Section S0, SI

$$w_{\text{Z}} = 2a_v + b_x \leq W \quad (3)$$

Model Code 2010 [8] – Control Section S0*

$$w_{\text{MC}} = 2a_v + 2b_y + b_x - 2d \leq W \quad (4)$$

German [10] Control Section S0

$$w_{\text{H240}} = t_{\text{x}} + 0{,}3\,(a_v + b_{\text{y}}/2) \leq W \quad (5)$$

$$t_{\text{x}} = b_{\text{x}} + 2t_{\text{p}} + t$$

$$t_{\text{y}} = b_{\text{y}} + 2t_{\text{p}} + t$$

$$0{,}2s < a_v < s,$$

$$0{,}2s < t_{\text{x}} \leq 0{,}4a, t_y \leq 0{,}2s$$

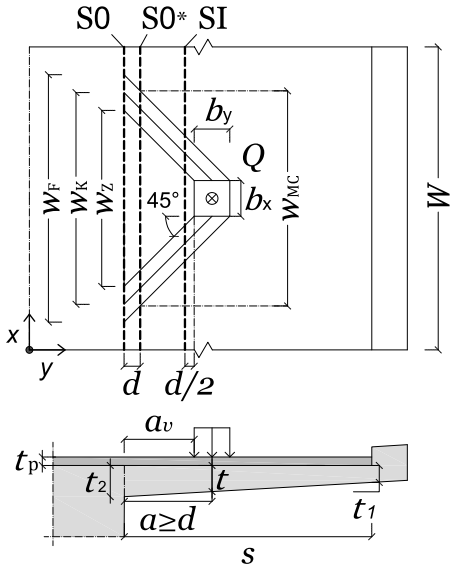

Figure 4 – Calculation of shear effective widths (w_{eff}). S0 is control section based on [8]*

Reissen & Heger [3, 11] performed tests on simple supported slabs varying W from 0.5 to 3.5 m. The specimens had a height (t) of 0.28 m and a/d of 4.2. According to [12], the slab with W=0.5 m was considered as beam, while the rest were slabs. Load-deflection (Q-u) and normalized shear-deflection (Q/W- u) curves were presented (Figure 5). The former shows how V increases with W (identifying V as Q_{exp}). The latter indicated that this increase was proportional to W for short specimens but started to decline for larger ones. Thus, a threshold value identified as w_{eff} was presumably between 1.5 m and 2.5 m, which could indicate the transition beam-to-slab behaviour.

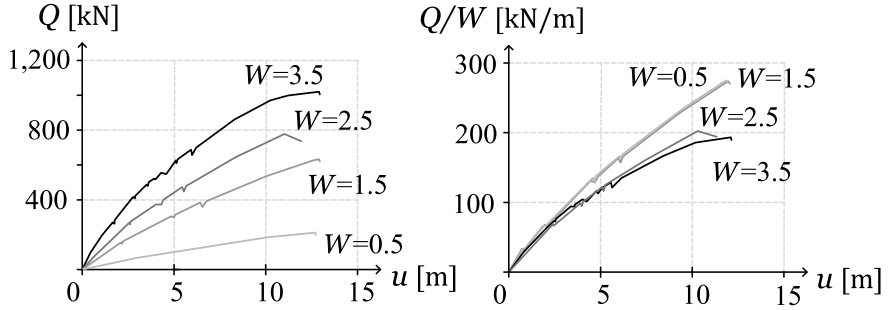

Figure 5 – $Q-u$ and $Q/W-u$ curves indicating the increased V with W. Replicated from [3]

In fact, in slabs of W≤1.5 m, the bottom flexural cracks developed nearly parallel to the support. The principal compressive stresses were constant and parallel to the span direction displaying an even load distribution over the whole W. In contrast, for W≥2.5 m, the flexural cracks at the

bottom propagated towards the support and no shear cracks at the lateral surfaces were observed until the ultimate load was exceeded. The inclination of the principal compressive stresses and their decrease of magnitude with the transversal distance from the load implied a slab behaviour. The value of w_{eff} was assessed from the experiment using Eq. 6 (w_{exp}) against some of the formulae above (Figure 6a). Note that these last ones were limited by the specimens' W. Q_{exp} is the failure load from the test, V_{G} is the dead weight of the load structure and v_{g} the self-weight of the specimen. The intermediate Dutch-French w_{K} had a good agreement whereas the Dutch w_{Z} and German w_{H240} turned out to be too conservative. It was however remarked that w_{K} could still lead to an underestimation since w_{exp} was above the line in the widest specimen. Given a constant d, the influence of a varying a in the slab of W=3.5 m was also analysed. Lower a/d led to higher w_{exp} (Figure 6b), which questioned the formulation for w_{eff} for loads close to the support.

$$w_{\text{exp}} = \frac{Q_{\text{exp}} + V_{\text{G}}}{v_{\text{Rd}} - v_{\text{g}}} \tag{6}$$

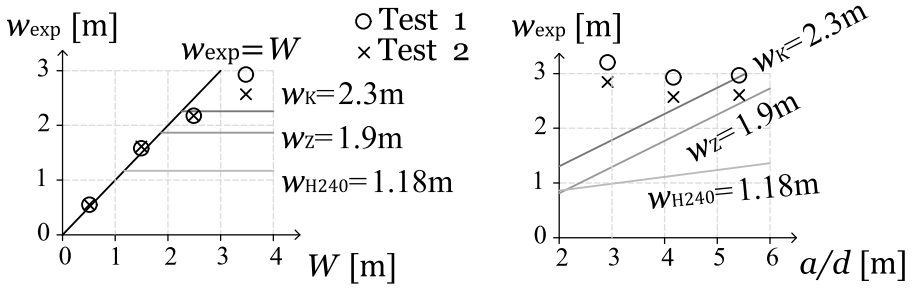

Figure 6 – a) w_{exp} vs w_{eff} based on different formulations. b) w_{exp} vs a/d. Replicated from [3]

Reissen & Hegger [5, 13] did experimental tests on overhang slabs of s=1.8 m with W=0.5 m and W=3.5 m. For each case, a constant height t=0.28 m and a tapered one from 0.28 m to 0.12 m were considered. Q_{exp} for W=3.5 m became approximately four times higher than for W=0.5 m, in both cases. However, no further tests with 0.5≤W≤3.5 or W≥3.5 m were performed, thus not being possible to draw a curve following Figure 2. Hence, the discussion of the influence of the W on V of overhang slabs and the location of the threshold remained open. The suitability of the formulation for w_{eff} was also investigated in these tests together with previous ones in the literature [2, 14]. Diagrams were presented showing Q_{exp} (including the self-weight) versus the theoretical shear load capacity (Q_{Rd}) calculated according to Eq. 7. w_{eff} was derived based on Figure 4. The intermediate French-Dutch effective width w_{K} turned out once again to have a good agreement even though in some cases it fell on the unsafe side (Figure 7).

$$Q_{\text{Rd}} = w_{\text{eff}}\,(v_{\text{Rd}} - v_{\text{g}}) \tag{7}$$

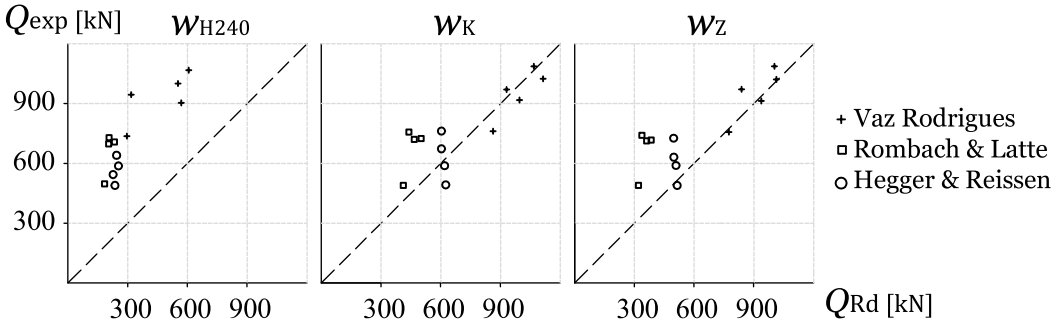

Figure 7 – Q_{exp} vs Q_{Rd} using different formulations for w_{eff}. Replicated from [5]

Reissen & Hegger & Classen [15] studied 34 tests on RC slabs and slab strips with $W \leq 3.5$ m. The internal redundancy of wide slabs yielded a more ductile shear failure than the comparatively brittle failure of slab strips. A decreasing shear slenderness enhanced moreover this ductility and allowed for arching action between the load and the support, which increased v_{Rd} significantly. The expression of Eurocode [6] addressing this case still resulted in conservative predictions.

Lantsogth [4] performed tests on slab strips with a total length of 5 m and t=0.3 m with continuous and simple supports. W varied from 0.5 to 2.5 m with a/d values of 1.51 and 2.26. The borderline between beam and slab was defined at $5t$ [6]. An increase of W resulted in an increase of Q_{exp} until a threshold was reached, where larger W would no longer lead to larger Q_{exp}. Two trend lines for each test that characterized the initial increase of Q_{exp} – in the shorter slabs – and the posterior almost constant Q_{exp} – in the wider slabs – were shown (Figure 8). The intersection between them was identified as w_{eff} which was compared to the French w_{F} and the Dutch w_{Z}. The most adequate was w_{F}, although it could be overestimated for increased a/d which influences its calculation. This brings up again the discussion concerning the suitability of the formulae for w_{eff} related to the geometry of the specimen, but in this case due to high values of a/d. The continuous support distributed less than the simple support, which might be non-conservative for w_{F}. Thus, different boundary conditions should be considered separately.

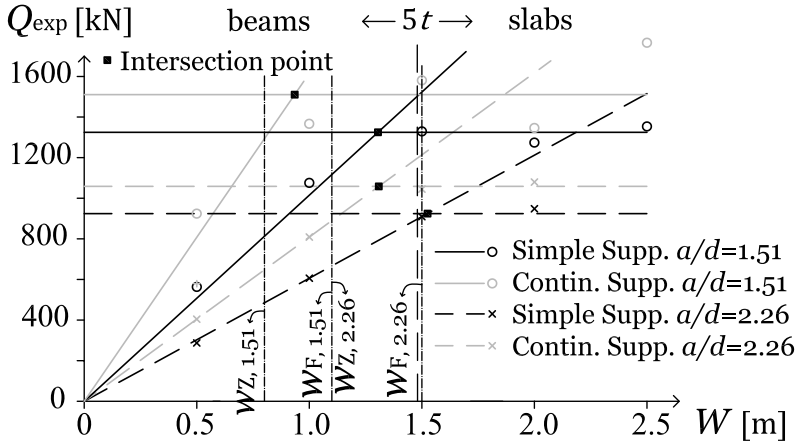

Figure 8 – Q_{exp} vs W and comparison of w_{eff} with intersection points. Replicated from [4]

Lantsoght [16] showed as well that shear trajectories developed neither parallel nor radially which indicated that one- and two-way shear failure modes could not be treated independently. The addressed differences between them were the influence of flexure, the effect of W and the crack location. Measurements of the force increments on reinforcement bars showed the essential connection between the two shear failure modes. For the transition zone between one- and two-way shear it was proposed to use one-way shear limited to w_{F} at the studied cross section.

Rombach & Henze [17] performed tests with t=0.25 m, W=4.5 m and s=1.9 m with different load positions (a) for one concentrated load. Similar Q_{exp} were obtained if $3d<a<6d$. This might question the use of w_{eff} because a load further from the root did not imply a better distribution. However, it could also be argued that the specimen's W might have been too short for that effect. For $a<2d$, Q_{exp} increased considerably because of an arch effect (direct compression strut).

3. METHODOLOGY

In order to study the influence of W on V of overhang slabs with and without an edge beam, the experimental tests DR1a and VK2V1 carried out by Rombach&Latte [14] and Vaz Rodrigues [2] respectively were used as references. DR1a was a tapered slab under four concentrated loads whereas VK2V1 was a flat slab under one concentrated load. None of them had an edge beam. The behaviour at ULS was investigated using a 3D non-linear FE-model with solid elements. Once the numerical results were validated against the experimental tests, the FE-model was extended to include different W according to Table 1 to determine its influence on V. All cases were considered slabs according to the Eurocode 1 since W>$5t$ [6]. An additional case based on VK2V1 was defined by moving the load 0.4 m towards the free edge. It was denoted as VK2V4 to respect the test labelling used. Finally, a fictitious edge beam was included in all simulations to quantify its influence on V. All load cases are presented in Figure 9. ABAQUS CAE and Explicit are used to generate the input file and to perform the non-linear FE-analyses, respectively.

Table 1 – Features of the simulations based on DR1a and VK2V1. CS denotes the central strip (addressed later). E denotes the width (W) of the original experiment. ρ stands for the transversal reinforcement ratio (top and bottom).

	W (m)	s (m)	W/s	t (m)	$5t$	ρ_{top}	ρ_{bot}
DR1a	10 – E	2.78	3.6	0.38-0.19	1.9	0.96	0.29
	7.5		2.7			0.73	
	4.2 – CS		1.5				
VK2V1	2.4 – CS, E	1.65	1.5	0.25	1.3	1.16	0.52
	4.5		2.7				
	10		6.1				

3.1 Description of the FE-model

General assumptions and limitations

Bond slip between concrete and reinforcement will influence the crack spacing. However, since no anchorage failure was reported in the tests and the aim of the numerical model was to predict the failure load, bond slip was not considered. The fluctuation of the load magnitude applied onto each plate during the experiment was not considered. The same load on each loading plate on the overhang was assumed. The initial load cycling in test DR1a has not been considered. A load-displacement curve for the FE-model comparison excluding this effect presented was used [2].

Geometry and reinforcement

The geometry of the models followed the experiments (Figure 9). For DR1a, the total length was 4.2 m, W was 10 m and s was 2.78 m. It had a tapered t from 380 mm at the root of the overhang to 190 mm at the free edge. The longitudinal reinforcement consisted of two layers (top and bottom) of ø12 mm bars with a spacing 150 mm. The transversal reinforcement was composed of ø16 mm bars with a spacing 75 mm, except for the last 1.4 m of the overhang span where the spacing was 150 mm. For VK2V1, the total length was 5.68 m, W was 2.4 m and s was 1.65 m. It had a constant t of 250 mm. The longitudinal reinforcement consisted of two layers (top and bottom) of ø12 mm bars with a spacing 100 mm. The transversal reinforcement was composed of ø16 mm bars with a spacing 80 mm at the top and ø12 mm bars with a spacing 100 mm at the bottom. In both tests, an edge beam of 400x400 mm^2 was added at the free edge of the slab according to Figure 9. The longitudinal reinforcement consisted of ø16 mm bars, and the transversal one is ø10 mm with a spacing 300 mm.

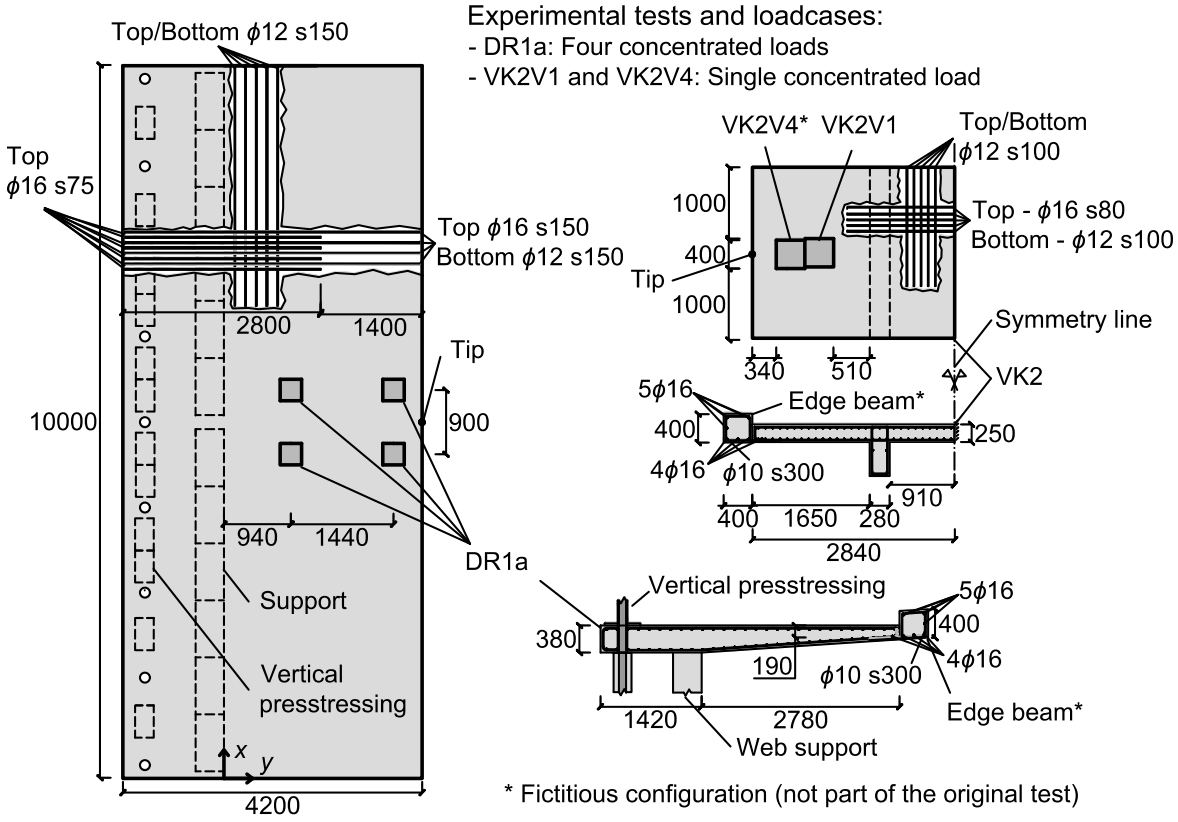

Figure 9 – Experimental test DR1a and VK2V1 (including fictitious case VK2V4 and the addition of edge beams). Only half of test VK2 is represented. Units in mm.

Material properties and models

The mechanical properties of concrete were based on the tests. The material model chosen was 'Concrete Damaged Plasticity' [18, 19] with default parameters values under multiaxial stress state. The tensile constitutive model consists of a linear-elastic branch until the tensile strength and a post-peak behaviour in terms of stress versus crack opening [20]. The fracture energy was calculated according to Model Code 2010 [8]. The compressive constitutive model was based on the uniaxial compression tests and adapted to the provisions of Eurocode 2 [6]. A linear-elastic behaviour was assumed up to 40% of the compressive strength followed by a parabolic approximation for the compression hardening and softening. The material model chosen for the reinforcement was 'Plastic' which allowed plastic isotropic hardening after yielding.

For DR1a, the concrete had a compressive strength of 39.1 MPa, tensile strength of 2.9 MPa and Young's modulus of 36.0 GPa. The reinforcement had a Young modulus of 200.0 GPa, yield strength of 499.0 MPa and ultimate strength of 600.0 MPa for the ø16 mm; and yield strength of 541.0 MPa and ultimate strength of 629.0 MPa for the ø12 mm and ø10 mm. For VK2 the concrete had a compressive strength of 46.0 MPa, tensile strength of 3.4 MPa and Young's modulus of 34.0 GPa. The reinforcement had a Young modulus of 195.0 GPa, yield strength of 550.0 MPa and ultimate strength of 607.0 MPa for the ø12 mm and ø10 mm; and yield strength of 554.0 MPa and ultimate strength of 646.0 MPa for the ø16 mm.

Mesh size and non-linear analysis procedure

For the non-linear analyses, a mesh of 8-noded solid elements with a characteristic element size of 25 mm was used for the concrete. This enabled at least eleven elements across t which is

suitable to describe non-linear shear behaviour. The reinforcement was modelled using truss elements. An explicit procedure in order to avoid convergence issues was used. The loading step was smoothed using a predefined function to avoid inertial forces affecting the results. Since the problem is quasi-static, the total and kinetic energy of the model during the simulation was monitored to ensure the accuracy of the analysis.

Loading, boundary conditions and constraints
The load was applied using a statically determinate structure built of beams and trusses connected to the loading plates, following the recommendations in [21]. A prescribed displacement-control was assigned to a node at the top of the structure and the reaction force was then determined. The web support was modelled by restraining all the degrees of freedom of the bottom surface. For the pre-stressing for test DR1a all the degrees of freedom at the two contact surfaces of the slab were restrained. Fully bonded reinforcement was assumed by constraining the nodes of the truss elements to follow the displacement degrees of freedom of the surrounding concrete.

3.2 Model validation

A comparison between the test and the FE-model concerning load-deflection $Q-u$ curves and failure mechanisms is shown in Figure 10. The displacement in the diagrams corresponds to the tip of the cantilever located at the symmetry axis with respect to the load application, as depicted in Figure 9. For test DR1a the difference in the initial stiffness between the test and the FE-model was a result of the initial cyclic loading performed in the experiment which was not included in the numerical analysis. A shear failure mode was observed in both cases in agreement with the experimental tests. The results presented were considered accurate enough to validate the FE-models in order to investigate overhang slabs of varying W, with and without an edge beam.

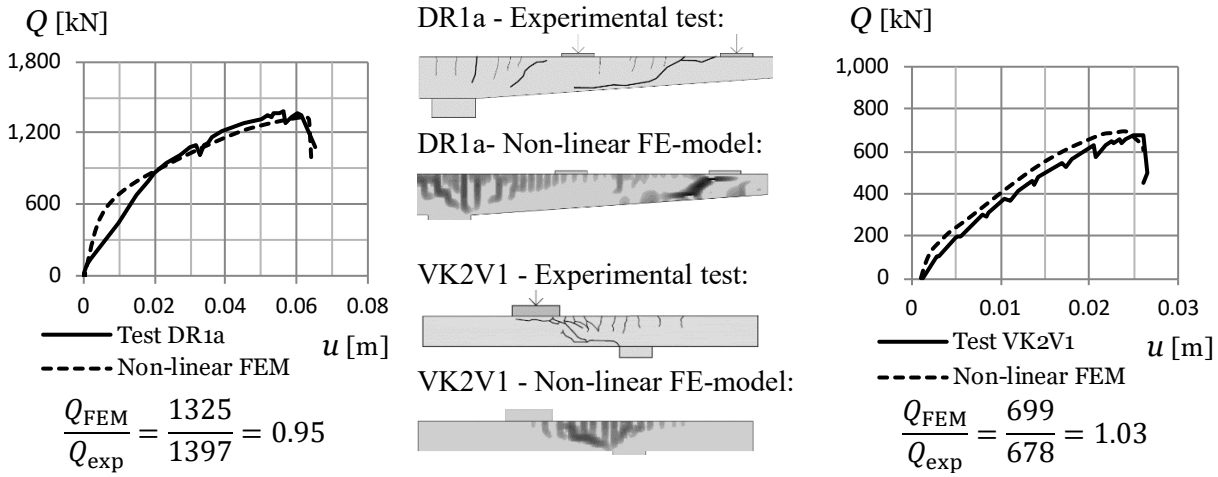

Figure 10 – $Q-u$ curves and crack pattern at failure for DR1a and VK2V1

4. RESULTS

This chapter presents the results of the non-linear FE-analyses. The control sections considered for shear failure were at the root and at a distance $d/2$ from the load. This resulted in three cross sections (S0, SI and SII) for DR1a corresponding to each load position and two (S0 and SI) for each VK2V1 and VK2V4 (Figure 11). These were assumed the same for the both cases, without and with an edge beam. For bending, the control section was either located at the root or at a change of flexural reinforcement for test DR1a. Each overhang was divided into strips, one central

and two lateral (Figure 11). The central strip (CS) for VK2V1 and DR1a matched W of the narrowest simulation, that is, 2.4 m and 4.2 m, respectively, in order to have a similar W/s ratio. The remaining parts at both sides from CS for increased W were regarded as lateral strips (LS).

The study focuses on the increase of V associated with W. Note that in the following text, V is identified as Q_{FEM}. The assumption is that this increase occurs because of (i) the redistribution of the shear forces from the concentrated loads and (ii) the increased shear capacity of concrete. The former was studied by determining the percentage of the shear force out of the total transferred through CS and LS during the loading sequence. For the latter, the ratio between the maximum shear forces transmitted through the CS in specimens with different W was evaluated at the failure cross section. The shear forces of each strip at the studied cross-sections according to Figure 11 were extracted with the tool NFORC of ABAQUS.

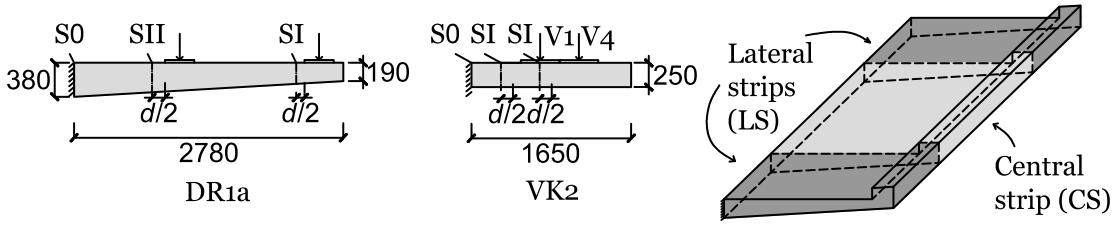

Figure 11 – Shear control sections for DR1a and VK2 and sketch of CS and LS. Units in mm.

The influence of W was studied for the slabs with/without edge beam excluding the self-weight. The reason for neglecting the dead load was to just analyse the shear force distribution from concentrated loads and draw conclusions without the impact of other loading. The results without the edge beam are presented first to understand the influence of only the increase of W. Then, the outcome concerning the effect of an edge beam is showed. The ultimate load from the simulation (Q_{FEM}), shear force distribution, shear capacity, failure mode, crack pattern and w_{eff} are addressed. Table 2 shows w_{eff} for the analysed slabs, limited to the specimen's W. A parameter z/d_1 is defined to document the proximity of the edge beam, where z is the distance from the load to the edge beam and d_1 is the effective depth at the connection of the slab and the edge beam.

Table 2 – Shear and edge beam span ratios, and w_{eff} in m for tests DR1a and VK2V1-V4

		DR1a			VK2V1			VK2V4		
	a/d	2.8 / 7.0			3.3			5.1		
	z/d_1	13.0 / 2.8			4.3			2.5		
	$W \rightarrow$	**4.2**	**7.5**	**10**	**2.4**	**4.5**	**10**	**2.4**	**4.5**	**10**
$w_{\mathrm{eff}} \rightarrow$	w_{Z}	4.2	6.3		2.2			2.4	2.7	
	w_{K}	4.2	6.0		1.8			2.4	2.5	
	w_{D}	4.2	5.7		1.4			2.2		
	w_{MC}	4.2	5.3		1.5			2.3		
	w_{H240}	2.12			0.9			1.0		

4.1 No self-weight, no edge beam

Rombach & Latte (VK2V1 and VK2V4)

Since no self-weight was included and the section was constant, any cross-section could be postulated as critical in shear. However, the bending moment across the span varied, which could influence the collapse and its location. In the simulations, all the specimens failed in shear at S0, with a high bending degree for VK2V4 as shown in the $Q-u$ curves (Figure 12).

Ultimate load Q_{FEM}

- Table 3 shows that Q_{FEM} increased with W significantly from 2.4 m to 4.5 m, namely 57% in VK2V1 and 41% in VK2V4. From 4.5 m to 10 m this increase was lower in VK2V1 (20%) and VK2V4 (22%) but still relevant, showing that Q_{FEM} could increase further if W>10 m.

Shear force distribution

- For W of 4.5 m and 10 m the shear force distribution to the sides compared to 2.4 m ranged 7-16% and 11-22% respectively for test VK2V1, and 12-20% and 17-49% respectively for test VK2V4 (Figure 13). An initial linear-elastic distribution followed by two stages of shear redistribution could be distinguished. The former occurred when the first bending cracks formed. From there, the force redistribution to the lateral strips started to grow smoothly with the load. The latter happened close to the peak load when the slope of this redistribution growth suddenly became steeper. The shear crack started to develop and the overhang displayed a ductile behaviour until failure. This second stage was especially remarkable in VK2V4 with W=10 m but barely noticeable in VK2V1 due to a more brittle collapse.

Shear capacity

- For W of 4.5 m and 10 m the shear capacity at S0 compared to 2.4 m increased 37% and 45% respectively for VK2V1, and 14% and 12% for VK2V4 respectively (Table 3). The difference in magnitude between VK2V1 and VK2V4 could be attributed to an arching effect due to the proximity of the load to the clamped edge. This effect, together with a reduction in the bending moment, enhanced the shear capacity. For 4.5 m and 10 m, the shear capacity of CS in both series remained nearly the same.

The increase of the shear capacity at S0 was the major contribution to the increase of V related to W for VK2V1, whereas the shear force distribution sideways was the one for VK2V4. For VK2V1 the rationale was the relatively low value of the bending moment and the arching action; for VK2V4 the increased W enabled a wider distribution for a load far from the root.

Failure mode, crack pattern and shear effective width w_{eff}

- In both 2.4 m specimens the shear crack spanned across the whole W at failure. For VK2V4 it inclined more towards the support than in VK2V1 because of the different load positions. Flexural cracks developed as well across the whole W parallel to the root (Figure 14a and Figure 15a) which indicated an activation of the full section and suggested a beam behaviour.
- For 4.5 m specimens the flexural cracks were still parallel to the root but they moved forward surrounding the load (Figure 14b and Figure 15b). In contrast, in the 10 m slabs the flexural cracks rotated towards the longitudinal free edge (Figure 14c and Figure 15c). The shear crack did not span across the whole W neither for 4.5 m nor for 10 m.
- Thus, the threshold w_{eff} should be located between 4.5 m and 10 m, probably closer to 4.5 m because of the transition observed in the flexural cracks and the trends shown in Figure 12. Certainly w_{eff} would be higher for VK2V4 than VK2V1 because of the load position. From this value, a slab behaviour would increasingly occur with more accentuated shear force distribution in the longitudinal direction and amplified ductility prior to failure.

Vaz-Rodrigues (DR1a)

Due to the tapered overhang, SII and, especially, SI were likely to be the critical sections for shear. A flexural failure could also be expected either at S0 or at the change of flexural reinforcement because of the eccentric loading. In the simulations, the 4.2 m specimen had a flexural failure

whereas the 7.5 m and 10 m ones failed in shear at SI (Figure 16). This reflected the influence on the failure mode of a reduced bending moment due to the increase of W.

Ultimate load Q_{FEM}

- Table 4 shows that Q_{FEM} increased with W compared to 4.2 m 16% and 17% for 7.5 m and 10 m, respectively. From 7.5 m to 10 m, the increase was only 1%, which shows the threshold should be 7.5 m or less in this case (Figure 16). This increase was much softer than for the VK2 slabs, perhaps because the failure mode in DR1a series was more localized.

Shear force distribution

- For all the specimens the shear force distribution to the sides at failure section SI were of 12% and 14% for 7.5 m and 10 m, respectively, in the linear-elastic stage (Figure 17). After that, an increase up to 19% and 21%, respectively, was observed when the first bending cracks developed. This increase softened during the loading due to internal redistribution until failure. These results proved that at SI, in spite of the proximity to the load application, there was room for further shear distribution sideways compared to shorter slabs.

Shear capacity

- For W of 7.5 m and 10 m the shear capacity of CS at SI increased 24% and 25% respectively. This showed the influence of a reduced bending moment compared to 4.2 m (Table 4). No arching effect occurred, which was logical given that the loads were not very close to the root.

Both the increase of the shear capacity of the section – because of the reduction of the bending moment – and the shear force distribution sideways associated with higher W were identified as the major contributions to the increase of V.

Failure mode, crack pattern and shear effective width w_{eff}

- Although the increase of Q_{FEM} was not as considerable as in the case of VK2 tests, the failure mode was influenced by W. The slab with 4.2 m failed in flexure. In contrast, 7.5 m and 10 m slabs failed in shear at SI in spite of a high bending degree. To evaluate if there would be a threshold for w_{eff} at SI is difficult because no significant increase of Q_{FEM} from 7.5 m and 10 m was observed (Figure 16) and the failure was localized around the load application.
- The shear crack at failure for slabs of 7.5 m and 10 m developed locally at SI but did not expand towards the free edge. In both cases, a secondary shear crack also developed close to the position of the other two loads, as documented in the real test [2]. The flexural cracks for W of 4.2 m at S0 were parallel to the root and spanned along the whole W, which suggested a beam behaviour (Figure 18a). A secondary relevant flexural crack in between the pair of loads developed in all the simulations because of the change of transversal reinforcement ratio. This crack went across the whole W for specimens of 2.4 m and 7.5 m, but not for 10 m. From this crack and with increasing W, the flexural cracks emerging around the two loads furthest from the root tended to propagate towards the longitudinal free edge (Figure 18b). In the case of 10 m, this affected even those flexural cracks that developed close to the root (Figure 18c). This tendency suggested therefore a local transition from beam to slab behaviour.

4.2 No self-weight, edge beam

Rombach & Latte (VK2V1-EB and VK2V4-EB)

A similar argument as the case without the edge beam could be argued for the cross section studied in shear. However, the reduction of bending moment is more relevant because of the edge beam

and may affect the failure. In fact, although both 2.4 m and 5 m specimens failed at S0, the 10 m ones collapsed at SI instead. Stiffer behaviours were also documented (Figure 12).

Ultimate load Q_{FEM}

- Table 3 shows that Q_{FEM} generally increased with the presence of an edge beam. The increase with W for VK2V1-EB of 2.4 m and 4.5 m compared with the slabs without an edge beam was of the same order (8-9%). For 10 m, the increase was not relevant (2%) because of the change of failure section. For VK2V4-EB of 2.4 m, the increase of Q_{FEM} due to addition of an edge beam was almost negligible. The edge beam deflected like a rigid solid and had no significant contribution to V. However, for 4.5 m and especially 10 m the edge beam could actually deform which provided additional stiffness and distributed the shear forces. This resulted in an increase of Q_{FEM} of 10% and 15% respectively and reflected the importance of the proximity of the edge beam to the load in wider overhangs.

Shear force distribution

- For 4.5 m and 10 m specimens the shear force distribution to the sides ranged 11-24% and 15-22%, respectively, for VK2V1-EB, and within 18-45% and 26-46%, respectively, for VK2V4-EB (Figure 13). The growth of the contribution of LS became more accentuated than without the edge beam. The linear-elastic branch of LS increased 5% and 10% for VK2V1-EB and VK2V4-EB, respectively. For 4.5 m cases, the edge beam also enhanced the ductile behaviour prior to failure since the second redistribution of shear forces was enabled, especially for VK2V4-EB. In contrast, for 10 m specimens a more brittle and stiffer behaviour was displayed than without the edge beam. The rationale was that, even though a shear crack started to form at the root, the shear failure took place at CSI (Figure 14f and Figure 15f).

Shear capacity

- For W of 4.5 m and 10 m the shear capacity of concrete compared to 2.4 m increased 24% and 42%, respectively, for VK2V1-EB, and 4% and 19%, respectively, for VK2V4-EB (Table 3). For VK2V1-EB the results smoothed compared VK2V1 because of the shear distribution along the edge beam. For VK2V4-EB of 4.5 m, no significant increase was observed which could support the fact that is in transition from beam to slab behaviour, in contrast to 10 m.

The edge beam was identified as the major contribution for the increase of V associated with W, especially for VK2V4-EB, since it contributed to an enhanced shear force distribution through this member. It is important to note that this distribution of shear forces occurs in such a one-way manner that part go to the overhang´s clamped edge and the remaining to the edge beam. These latter are transferred back to the slab across the length of the edge beam, as explained later on.

Failure mode, crack pattern and shear effective width w_{eff}

- The failure cross section was located at S0 for 2.4 m and 4.5 m specimens. The 2.4 m specimens behaved similarly as without the edge beam, that is, the shear crack spanned across the whole W and flexural cracks were parallel to the root.
- For 4.5 m specimens, the flexural cracks did not move forward to the sides of the load as it happened without the edge beam. The shear crack did neither span along the whole W, but more ductility was exhibited than before. This was especially remarkable in VK2V4-EB where a crack along the inner side of the edge beam developed in the longitudinal direction of the overhang slab but without going through this member. This might explain the increased ductility before failure because the edge beam could still distribute force from the concentrated load although the shear crack was developing (Figure 14e and Figure 15e).

- For 10 m specimens the failure cross section shifted to SI. The collapse was brittle in contrast to 4.5 m. A reason could be that the bending moment at the root diminished because of the edge beam, thus allowing S0 to increase its shear capacity. An identified difference was that in VK2V1-EB the main shear crack developed further towards the root whereas in VK2V4-EB it did around the load, resembling a punching failure. In both tests, a secondary shear crack at S0 had formed earlier. The flexural cracks propagated from the root to the free longitudinal edge but the distribution angle became higher than without an edge beam. Thus, one-way shear behaviour was occurring (Figure 14f and Figure 15f). It is interesting to note that, in contrast to 4.5 m, longitudinal cracks through the edge beam took place.
- From the crack pattern and the failure mode, in a similar way as without the edge beam, the 2.4 m specimens displayed a beam behaviour whereas in the 4.5 m and 10 m specimens a slab behaviour was observed. In contrast, the presence of the edge beam altered the distribution of shear forces tending to one-way. Part of the shear forces went towards the root, while the rest did to the edge beam. These returned at the end of it to the slab to be further distributed to the root. The threshold w_{eff} could again be assumed to be between 4.5 m and 10 m, presumably higher for VK2V4 as the trend was steeper than without the edge beam (Figure 12).

Table 3 – Q_{FEM} and shear capacity ratios for VK2V1 and VK2V4 with and without edge beam

	W (m)	Q_{FEM} (kN)	$Q/Q_{2.4}$	$Q/Q_{4.5}$	$Q_{\text{EB}}/Q_{\text{nEB}}$	$CS/CS_{2.4}$	$CS/CS_{4.5}$
VK2V1	2.4	756					
	4.5	1,185	1.57			1.37	
	10	1,419	1.88	1.20		1.45	1.06
VK2V1-EB	2.4	819			1.08		
	4.5	1,286	1.57		1.09	1.24	
	10	1,445	1.76	1.12	1.02	1.42	1.15
VK2V4	2.4	641					
	4.5	905	1.41			1.14	
	10	1,108	1.73	1.22		1.15	1.01
VK2V4-EB	2.4	643			1.00		
	4.5	992	1.54		1.10	1.04	
	10	1,271	1.98	1.28	1.15	1.19	1.14

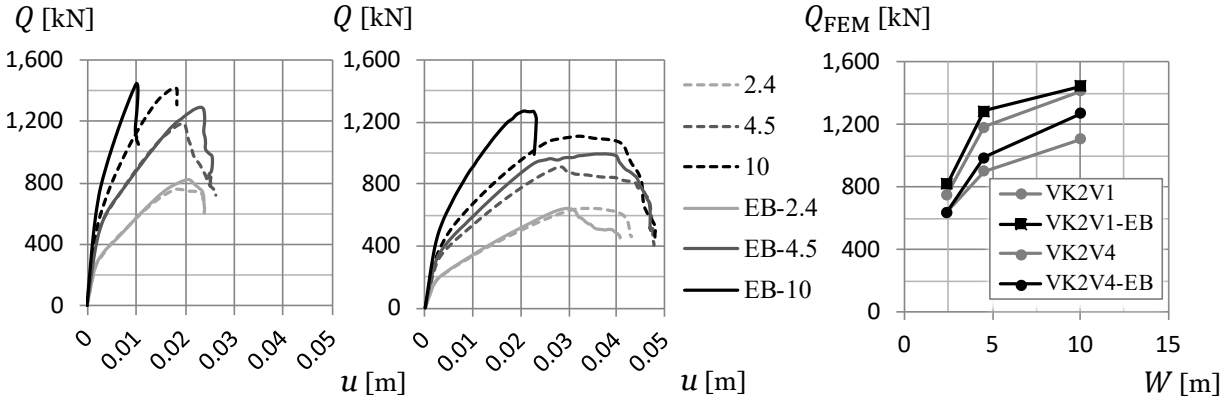

Figure 12 – $Q-u$ (left) and Q_{FEM} vs W (right) from non-linear FE-analyses for slabs VK2V1, VK2V1-EB, VK2V4 and VK2V4-EB.

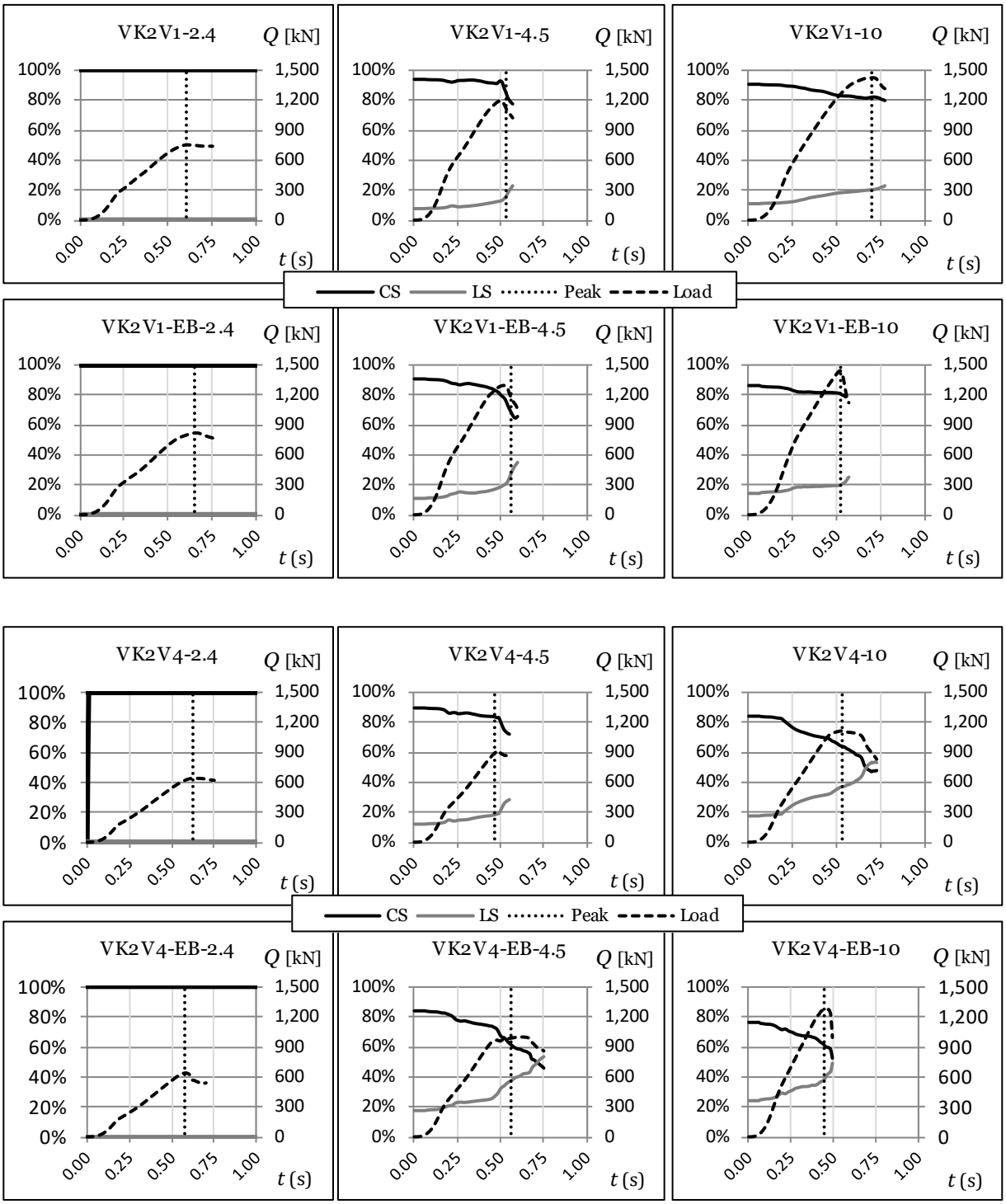

Figure 13 – Shear distribution for VK2V1 and VK2V4 with/without edge beam at S0 (root)

Vaz Rodrigues (DR1a-EB)

Similarly to the case without an edge beam, the specimen with 4.2 m had a flexural failure and both 7.5 m and 10 m slabs failed in shear at SI. The behaviour was, however, stiffer (Figure 16).

Ultimate load Q_{FEM}

- Table 4 shows that Q_{FEM} increased with W 13% and 21% compared to the slabs without the edge beam for 7.5 m and 10 m, respectively. It was however not relevant for the 4.2 m specimens (4%). The importance of W for DR1a-EB was also reflected because the 7.5 m and

10 m slabs had an increase of 27% and 36%, respectively, compared to the one of 4.2 m. From 7.5 m to 10 m, the increase was of 8%, which is considerably higher than in the tests without an edge beam and proves the additional contribution of this member.

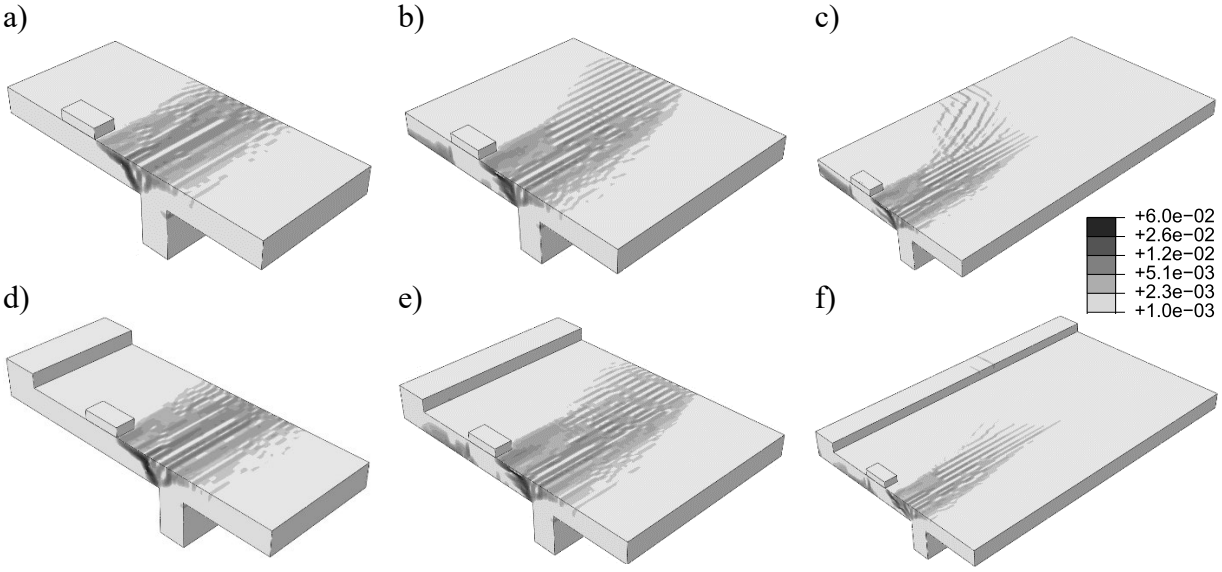

Figure 14 – Crack pattern for VK2V1 and VK2V1-EB at failure

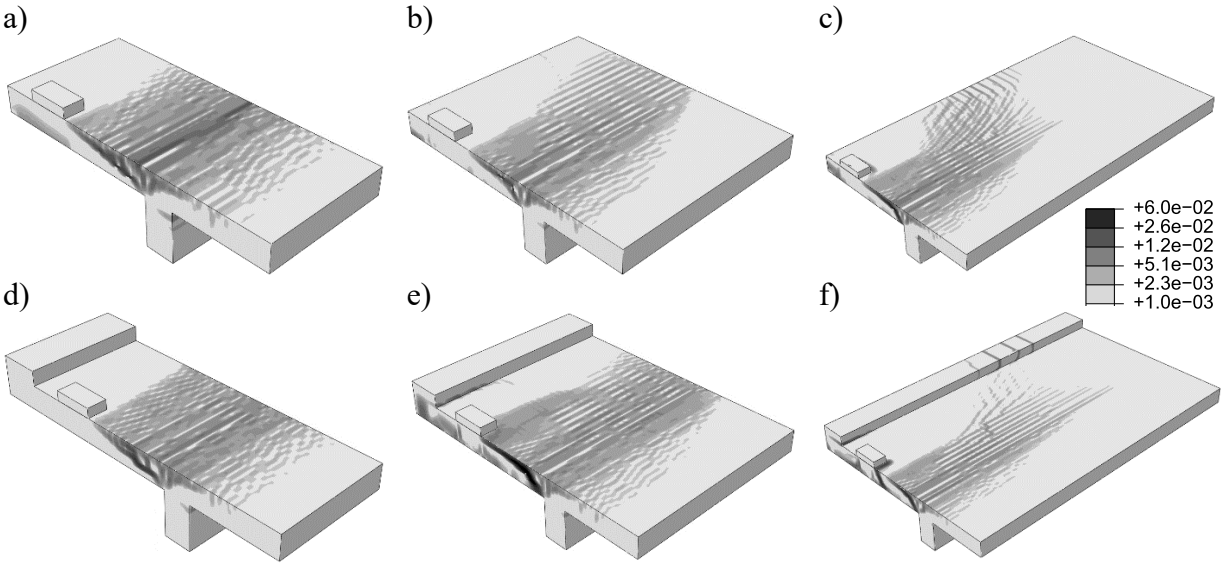

Figure 15 – Crack pattern for VK2V4 and VK2V4-EB at failure

Shear force distribution

- The shear force distribution to the sides at SI remained almost at a similar level for both DR1a and DR1a-EB of 7.5 m. For W of 10 m, it had an increase up to 26% (Figure 17). Thus, a greater load distribution took place transversally, especially due to the edge beam.

Shear capacity

- For W of 7.5 m and 10 m the shear capacity in the central strip of 2.4 m increased 28% and 35%, respectively, thus representing an increase compared to the specimens without the edge beam, especially for 10 m (Table 4).

The edge beam was identified as the major contribution to the increase of V together with W. This was especially relevant for the case of 10 m.

Failure mode, crack pattern and shear effective width w_{eff}

- The failure mode was influenced by W and the edge beam. The 4.2 m specimen had a flexural failure but in contrast to the slab without the edge beam, flexural cracks did not propagate to the longitudinal free edge (Figure 18d). Additional simulations performed by the authors with W=5 m showed that a flexural failure would occur without edge beam, but a shear one would take place if there were an edge beam, which reflected the impact of this member. For 7.5 m, a significant change of crack pattern compared to the test without the edge beam was observed (Figure 18e). Even though some cracking occurred at the end of the edge beam, the flexural cracks propagated mostly to the transversal free edge instead of the longitudinal one. For 10 m, a similar flexural crack pattern to VK2V1 was detected with the crack rotating towards the free longitudinal edge and propagating through the edge beam (Figure 18f).
- Concerning w_{eff}, in contrast with the slab without an edge beam the trend was not plane, and a smooth increase was observed (Figure 16). This would therefore support the fact that a threshold could instead be located between 7.5 m and 10 m.

Table 4 – Q_{FEM} and shear capacity ratios for DR1a with and without edge beam

	W (m)	Q_{FEM} (kN)	$Q/Q_{2.4}$	$Q/Q_{4.5}$	$Q_{\text{EB}}/Q_{\text{nEB}}$	$CS/CS_{2.4}$	$CS/CS_{4.5}$
DR1a	4.2	1,143					
	7.5	1,327	1.16			1.24	
	10	1,341	1.17	1.01		1.25	1.00
DR1a-EB	4.2	1,187			1.04		
	7.5	1,502	1.27		1.13	1.28	
	10	1,617	1.36	1.08	1.21	1.35	1.05

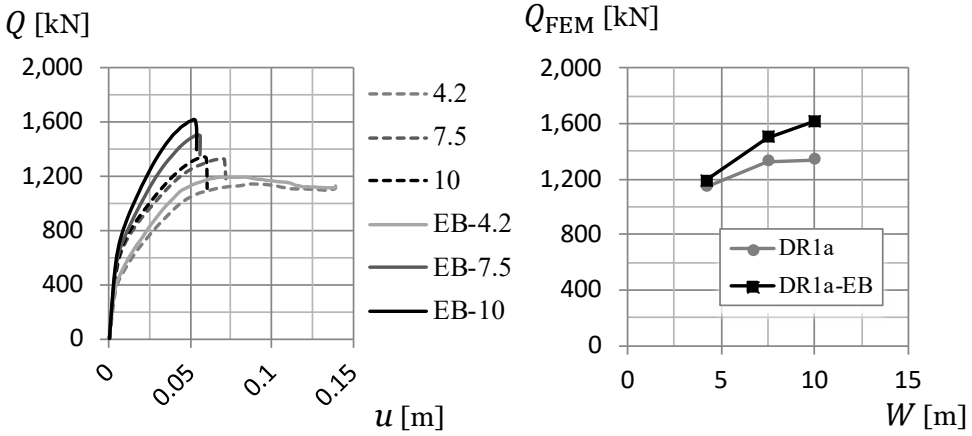

Figure 16 – $Q-u$ (left) and Q_{FEM} vs W (right) from non-linear FE-analyses for slabs DR1a and DR1a-EB

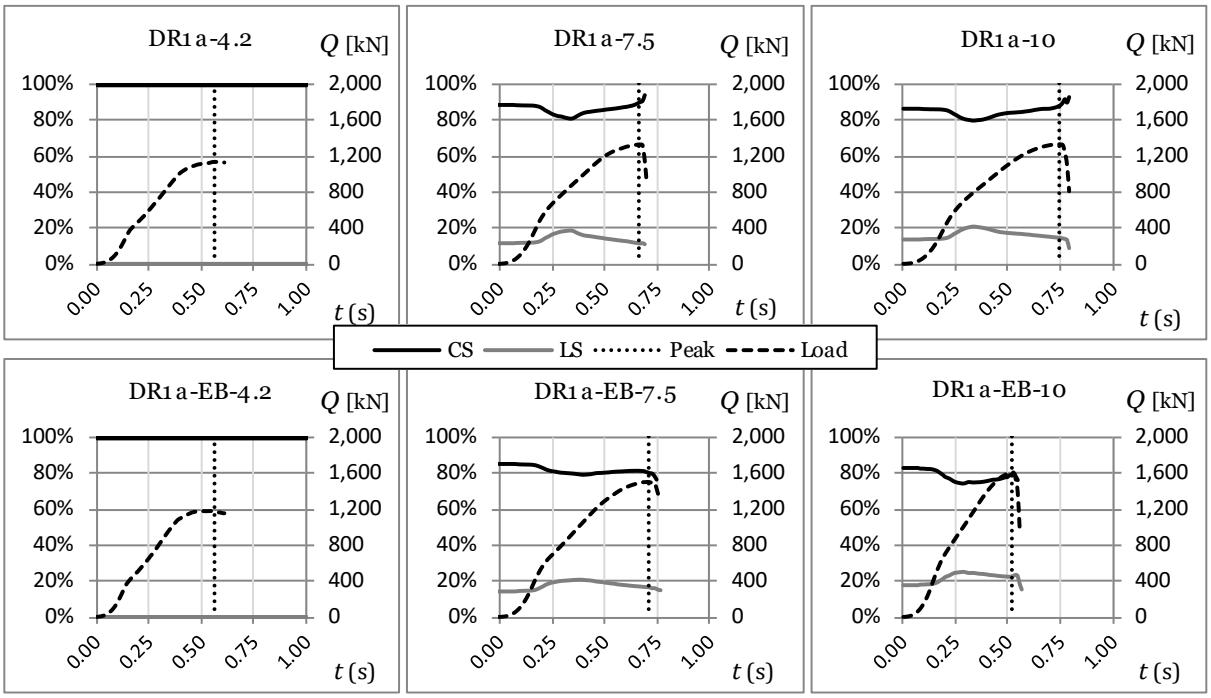

Figure 17 – Shear distribution for tests DR1a with/without edge beam at SII

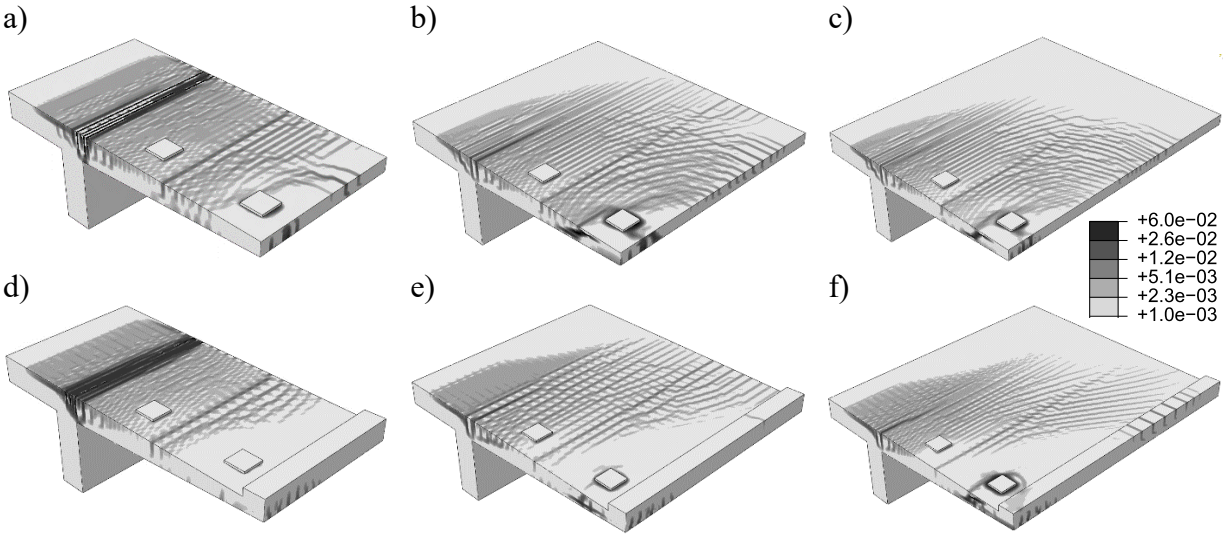

Figure 18 – Crack pattern for DR1a specimens at failure

4.3 Discussion

Influence of the width of the overhang (W)

The results reflect that the increase of the bearing capacity V of an overhang slab is associated with the increase of the width W. The location of the threshold value identified as the shear effective width w_{eff} that delimits this increase could be intuited from Figures 12 and 16. Thus, the shape of the relationship between V and W could be assumed as suggested by Figure 2. Design formulae for w_{eff} exist but lack the consideration of the total W, the support conditions or d, among other factors, which influence the structural behaviour.

In this article, the mechanisms behind the increase of V associated with W were identified as the distribution of the shear force in the longitudinal direction and the increase of the shear concrete

capacity v_{Rd}. The former was evaluated by the contribution of the lateral strip (LS) when W was enlarged. Its influence could initially be seen in the linear-elastic behaviour where the distribution of the shear force in LS had a slight increase with W. Subsequently, redistribution at a first stage from the central strip (CS) to LS occurred after the first flexural cracks at the root. This flow of forces grew with the load until the maximum peak was reached. Then, a second redistribution stage took place, which yielded a ductile behaviour prior to failure. This was mostly perceptible for VK2V4 where the load was located further from the overhang's root. The shear concrete capacity generally increased with W, significantly for a/d of 3.3 (VK2V1) which could be attributed to an arching effect.

Influence of the edge beam

The results corroborate the contribution of the edge beam to V of an overhang slab, especially for loads close to the free edge in line with previous findings [1]. This continued work including a new test showed a more effective influence of the edge beam for an increasing W, with further distribution of the shear forces. A parameter to account for the proximity to the edge beam z/d_1 was introduced. Values of 2.5 (VK2V4-EB) and 2.8 (DR1a-EB) should thus be noted for a contributing edge beam. Hence, the edge beam could be named as a third factor for the increase of V with W. The crack pattern and the strip analysis showed that there was a one-way distribution of forces, where part was transferred towards the root and the rest to the edge beam, being carried through it and returning back to the slab in the adjacent strips, as illustrated in Figure 19.

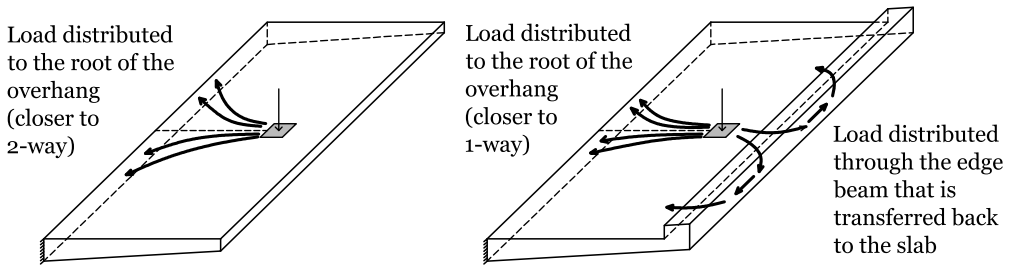

Figure 19 – Sketch of the distribution of shear forces from a concentrated load comparing an overhang slab with/without an edge beam.

Because of this distribution, the edge beam influences the collapse mechanism too. For a flat overhang with an edge beam, the increase of W implied that the failure cross section could be moved from the root to a section placed close to the load application, as it happened for VK2 tests. A higher V was achieved, but the shear failure was brittle, interrupting the second redistribution stage after the maximum load. This change of failure section could be attributed to an increase of the shear capacity of the root because of a reduced bending moment due to the edge beam.

In a tapered overhang slab under concentrated loads close to the free longitudinal edge, a critical cross section for shear failure could presumably be located near the load application because of the thinner d. However, the edge beam strengthens this section and an eventual shear failure could occur at the root or at other section close to other loads, as it was observed for DR1a. On the other hand, for shorter overhangs without an edge beam that would fail in flexure, the fact of adding this member may not only result in an increase of V but also change the collapse mechanism.

The cross section analysed and the shear effective width w_{eff}

Shear failure in overhangs can occur at the root (S0) or at a cross section near the load, typically at a distance of $d/2$ or $2d$ (SI). For S0, the results for VK2 tests showed a sideways redistribution of the shear force, which supports the suitability of the use of w_{eff} to study shear failure. In this

case W becomes paramount until the threshold value is reached. Ideally, the formulae for w_{eff} should match the threshold value but it was shown that higher Q_{FEM} were reached if $W>w_{\mathrm{eff}}$. Hence, these formulae should be revisited. If experimental tests are used for this purpose, the specimens should be wide enough to capture the real behaviour of a bridge overhang slab.

For the study of shear failure at SI the computed values of w_{eff} are low because of the limited possibility to spread the shear forces in contrast to S0. In this case, the influence of W might not be so significant at least for design purposes if an enough wide overhang slab is considered. If collapse occurs here, it is localized and more associated with a two-way shear failure. A three-sided control perimeter around the load could be used as w_{eff}. The edge beam is relevant for loads close to the free edge and this case should be covered in the design codes and calculation of w_{eff}.

For flexural failure, if ρ is constant, S0 should be analysed since the bending moment is maximum. Effective widths for the distribution of bending moments exist [1]. Cross sections located at a discontinuity in ρ should be investigated as well, as it was the case of DR1a.

5. CONCLUSIONS

The influence of the width of the overhang slab W on the load bearing capacity V was studied with the aid of validated non-linear FE-simulations using experiments from the literature. Such cases represent different geometries, reinforcement ratios ρ, loading setups and variable/constant effective depths d. Moreover, an edge beam was included to investigate the effect of this member with respect to those factors. The conclusions are the following:

- V of overhang slabs increases with W until a certain threshold value, identified as w_{eff}, is reached. The mechanisms behind this increase are the shear distribution and posterior redistributions sideways, and the increase of v_{Rd}. The distribution starts from the linear-elastic behaviour. The redistribution takes place from the formation of the first flexural cracks until the maximum load is reached, allowing for even further redistribution prior to failure.
- The edge beam also contributes to the increase of V of overhang slabs and its efficiency is dependent on W. The shear force distribution tends to be one-way towards both the root of the overhang slab and the edge beam, which transfers back those forces along the specimen.
- The load position becomes significant in relation to the aforementioned mechanisms and the structural behaviour of the overhang slab. For a load close to the root with low a/d the increase of v_{Rd} because of an arching effect is predominant while, for a load close to the free edge, the shear redistribution sideways has more weight especially in combination with an edge beam, considering low values of z/d_1.
- This quantitative effect also turns out to be qualitative as both W and the edge beam influence the collapse mechanism. Not only the cross section that becomes critical is influenced but the failure mode that can shift between shear and flexural as well.
- For the enhancement of current design codes for bridge overhang slabs, especially to determine w_{eff}, new experimental tests are needed. The increase of V with W and the influence of the edge beam should be factors to be accounted for in the planning of such tests.

6. ACKNOWLEDGEMENTS

The authors wish to express their gratitude to the Swedish Construction Industry's Organisation for Research and Development ('Svenska Byggsbranschens Utvecklingsfond', SBUF).

REFERENCES

1. Veganzones Muñoz JJ, Pacoste C, Pettersson L & Karoumi R: "Influence of Edge Beam on Behavior of Bridge Overhangs". *ACI Structural Journal*, Vol. 115, 2018, pp. 957-70.
2. Vaz Rodrigues R: "Shear Strength of Reinforced Concrete Bridge Deck Slabs". *Thesis* No. 3739 (PhD Thesis). École Polytechnique Fédérale de Lausanne, Lausanne, Switzerland, 2007.
3. Reissen K & Hegger J: "Experimental investigations on the effective width for shear of single span bridge deck slabs". ("Experimentelle Untersuchungen zur mitwirkenden Breite für Querkraft von einfeldrigen Fahrbahnplatten"). *Beton- und Stahlbetonbau*, Vol. 108, No. 2, 2013, pp. 96-103. (In German).
4. Lantsoght E O L, de Boer A, van der Veen C & Walraven J C. "Effective Width in Shear of Reinforced Concrete Solid Slab Bridges under Wheel Loads". *Proceedings*, TRB 93rd Annual Meeting Compendium of Papers, Washington DC, 2014, pp. 12-16.
5. Reissen K & Hegger J: "Experimental investigations on the shear-bearing behaviour of bridge deck cantilever slabs under wheel loads". ("Experimentelle Untersuchungen zum Querkrafttragverhalten von auskragenden Fahrbahnplatten unter Radlasten"). *Beton- und Stahlbetonbau*, Vol. 108 (5), 2013, pp. 315-324. (In German).
6. CEN [European Committee for Standardization]: "Eurocode 2: Design of concrete structures - Part 1-1: General rules and rules for buildings. EN 1992-1-1". Brussels, Belgium, 2005.
7. American Concrete Institute (ACI): "318-14 Building code requirements for structural concrete and commentary". Farmington Hills, MI, USA, 2014, 520 pp.
8. FIB: "Model code for concrete structures 2010". Ernst & Sohn, Lausanne, Switzerland, 2010.
9. Zanuy C & Gallego J M: "Discussion of Shear Design of RC Bridge Deck Slabs according to Eurocode 2 by Guenter Rombach and Matthias Kohl". *ASCE Journal of Bridge Engineering*, Vol. 20, No. 9, 2015.
10. DAfStb German Committee for Structural Concrete Book 240. "Tools for calculation of internal forces and changes in shape of reinforced concrete members." ("Deutscher Ausschuss für Stahlbeton Heft 240: Hilfsmittel zur Berechnung der Schnittgrößen und Formänderungen von Stahlbetonbauwerken"). Berlin, 1976-1991. (In German).
11. Reissen K & Hegger J: "Experimental Study on the Shear Capacity of Concrete Slabs". *Proceedings,* IABSE-IASS Symposium 2011, London, September 2011, pp. 584.
12. DIN German Design Code: "1045-1 Design and Construction of Concrete Reinforced Concrete and Prestressed Concrete". ("Bemessung und Konstruktion von Stahlbeton- und Spannbetonbauteilen"), Berlin, 2008. (In German).
13. Reissen K & Hegger J: "Experimental investigations on the shear capacity of RC cantilever bridge deck slabs under concentrated loads - Influences of moment-shear ratio and an inclined compression zone". *Proceedings.* 16th European Bridge Conference, Edinburgh, June 2015.
14. Rombach G & Latte S: "Shear resistance of bridge decks without shear reinforcement". *Proceedings*, fib Symposium, Tailor Made Concrete Structures, Amsterdam, May 2008, pp. 519-525.
15. Reissen K, Classen M & Hegger J. "Shear in reinforced concrete slabs—Experimental investigations in the effective shear width of one-way slabs under concentrated loads and with different degrees of rotational restraint". *Structural Concrete*, Vol. 19, No. 1, 2018, pp. 36-48.

16. Lantsoght EOL, van der Veen C, de Boer A & Walraven J C. ”Transition from one-way to two-way shear in slabs under concentrated loads”. *Magazine of Concrete Research*, Vol. 67, 2015, pp. 909-22.
17. Rombach G & Henze L: “Shear capacity of concrete slabs without shear reinforcement under concentrated loads close to support”. *Proceedings,* fib Symposium, Springer, Maastrich, June 2017, pp. 676-683.
18. Lubliner J, Oliver J, Oller S & Onate E: “A plastic-damage model for concrete”. *International Journal of Solids and Structures*, Vol. 25, No. 3, 1989, pp. 299-329.
19. Lee J & Fenves GL: “Plastic-Damage Model for Cyclic Loading of Concrete Structures”. *Journal of Engineering Mechanics*, Vol. 124, No. 8, 1998, pp. 892-900.
20. Cornelissen H, Hordijk D & Reinhardt H. “Experimental determination of crack softening characteristics of normal weight and lightweight concrete”. *Heron*, Vol. 31, No. 2, 1986, pp. 45-56.
21. Broo H, Lundgren K & Plos M. “A guide to non-linear finite element modelling of shear and torsion in concrete bridges”. *Report* 2008:18. Chalmers University of Technology, Dept. of Civil and Environmental Engineering, Gothemburg, Sweden, 2008, pp. 21.

LIST OF NOMENCLATURE

Roman lowercase	
a	Distance from the load center point to the root of the overhang
a/d	Shear-span ratio
$b_{\mathrm{x,y}}$	Width of the load (in the x- or y-direction)
d	Effective depth
d_1	Effective depth at the connection of the slab and the edge beam
s	Span of the overhang slab
t	Thickness of the slab
t_{p}	Thickness of the pavement
w_{eff}	Shear effective width, subtitle may indicate the formulation used for its derivation
u	Vertical deflection
z	Distance from the load to the free edge or the inner side of the edge beam
Roman uppercase	
Q	Applied load
Q_{exp}	Failure load in the experimental test
Q_{FEM}	Failure load in the numerical FE-simulation
Q_{Rd}	Theoretical shear capacity
V	Bearing capacity
V_{G}	Dead weight of the load structure (of the test)
W	Slab width
Greek lowercase	
ρ	Transversal reinforcement ratio
ν_{Rd}	Shear concrete capacity
ν_{g}	Self-weight of the specimen